Machine learning inversion approach for soil parameters estimation over vegetated agricultural areas using a combination of water cloud model and calibrated integral equation model

Sadegh Ranjbar,[a] **Arastou Zarei**,[a] **Mahdi Hasanlou**,[a,*] **Mehdi Akhoondzadeh**,[a] **Jalal Amini**,[a] **and Meisam Amani**[b]

[a]University of Tehran, College of Engineering, School of Surveying and Geospatial Engineering, Tehran, Iran

[b]Wood Environment and Infrastructure Solutions, Ottawa, Ontario, Canada

Abstract. Estimating volumetric soil moisture (M_v) and surface roughness (S) are the key parameters for numerous agricultural and hydrological applications. Although these two parameters can be effectively retrieved from synthetic aperture radar (SAR) data, the presence of vegetation can negatively affect the results. A method was proposed to accurately estimate M_v and S over vegetated agricultural areas. The method was based on applying the machine learning inversion approach along with SAR data to invert a combination of the parameterized water cloud model (PWCM) and the calibrated integral equation model (CIEM). The soil backscattered component in water cloud model (WCM) was generated by CIEM to be applied to the WCM parameterization and dataset simulation. Three machine learning algorithms, including the support vector regression (SVR), multi-output SVR (MSVR), and artificial neural network (ANN), were employed to model the relationship between the simulated dataset variables. The genetic algorithm was also applied to optimize the models' parameters. The inversion technique results demonstrated that the MSVR and ANN had the highest accuracy in estimating M_v and S due to their better structures. The SMAPVEX-16 *in situ* dataset, along with three Sentinel-1 images, was applied to evaluate the accuracy of the WCM parameterization and the proposed method for M_v and S estimation. The accuracies of the PWCM in the VV and VH polarizations of Sentinel-1 C-band data were reasonable for VWC < 2.5 kg/m^2 [root-mean-square error (RMSE) = 1.44 and 1.77 dB, respectively]. Additionally, it was observed that the trained SVR, MSVR, and ANN had similar results for different VWC values. In summary, the proposed method had high potential in vegetated agricultural areas with VWC < 2.5 kg/m^2, for which the RMSEs were 4 to 7 vol. % and 0.35 to 0.46 cm depending on the VWC values in retrieving M_v and S, respectively. © *2021 Society of Photo-Optical Instrumentation Engineers (SPIE)* [DOI: 10.1117/1.JRS.15.018503]

Keywords: remote sensing; machine learning; synthetic aperture radar; soil moisture; soil roughness; water cloud model; calibrated integral equation model.

Paper 200842 received Nov. 27, 2020; accepted for publication Feb. 18, 2021; published online Mar. 8, 2021.

1 Introduction

Volumetric soil moisture (M_v) and surface roughness (S) retrieval are important for various environmental studies, including hydrology,[1,2] climate change analysis,[3,4] natural resources management,[1,5] and precision agriculture.[2,6] The response of synthetic aperture radar (SAR) signals has been widely evaluated as a function of surface parameters in agricultural fields.[7–9] Many researchers have investigated the feasibility of retrieving soil parameters, such as M_v and S from airborne and spaceborne SAR systems.[10–12]

The SAR backscattering coefficient (σ^o) is a function of the physical and electrical characteristics of a target.[13] σ^o mainly depends on the characteristics of the surface and SAR sensor.[13,14] In

*Address all correspondence to Mahdi Hasanlou, hasanlou@ut.ac.ir

1931-3195/2021/$28.00 © 2021 SPIE

this regard, σ^o is significantly affected by M_v and S.[4,15] So far, many techniques and models have been proposed, verified, and validated to retrieve M_v and S from various SAR datasets.[13,16–18] The corresponding methods can be divided into three main categories: (1) theoretical models, (2) empirical regression techniques, and (3) semiempirical models.[19,20] For instance, the integral equation model (IEM) is one of the theoretical models that is commonly applied to estimate M_v and S through inversion techniques.[18,21,22] Compared to other existent models that usually can be applied to either smooth or rough surfaces, IEM enables to model S values with a broad range of values.[23–25]

M_v and S retrieval using SAR data with the presence of vegetation cover in agricultural areas is complicated because vegetation cover affects SAR backscattering values from soil.[26–28] The water cloud model (WCM) is utilized in many studies to model the vegetation impacts on σ^o and to estimate the soil parameters in the vegetated agricultural areas. Several studies have so far utilized WCM and discussed its advantages and limitations for soil parameters estimation the agricultural regions. For instance,[29] the WCM employed to simulate quad-polarization σ^o in the C-band with the incidence angle (θ) of 30 deg for wheat and pea fields. The root-mean-square errors (RMSEs) varied from 0.7 to 1.0 dB and from 0.2 to 1.2 dB depending on the crop type for the simulated cross polarization and co-polarization, respectively. Moreover,[5] developed an inversion approach for M_v retrieval using X-band SAR and optical data over agricultural areas. The best results were obtained with an RMSE of 3.6 to 6.1 vol. % for different NDVI values. Khedri et al.[30] also proposed the modified improved WCM as a semianalytical method to estimate M_v using PolSAR imagery. The results demonstrated that the proposed method had a high accuracy with the coefficient of determination $(R^2) = 95\%$ to 98% and RMSE $= 0.00012$ to 0.0016. Furthermore, Bao et al.[31] presented a new method for M_v estimation over sparse vegetation area based on a combination of SAR and optical data. A spectral index generated from the Landsat-8 imagery was utilized as a vegetation descriptor to eliminate the vegetation impacts on Sentinel-1 σ^o values. The correlation coefficient (r) and RMSE of 0.911 and 0.053 $\mathrm{cm}^3/\mathrm{cm}^{-3}$ were, respectively, obtained. Xing et al.[32] also used a modified WCM to eliminate the vegetation effects on σ^o. The validation against *in situ* measurements resulted in $R^2 = 71\%$ and RMSE $= 4.43$. Finally, Rawat et al.[33] estimated M_v over the agricultural fields by a modified WCM using a combination of SAR and optical satellite data. In this study, the model performance was validated for three days and the following results were reported: $R^2 = 86\%$, 96%, and 91% and RMSE $= 0.06$, 0.03, and 0.02 vol. %.

In IEM, σ^0 is determined as a function of the characteristics of the SAR system and soil parameters. Three parameters are generally employed as the descriptors of S in the bare agricultural field: (1) the standard deviation of heights (h_{rms}), (2) the correlation function, and (3) the correlation length (l). Several studies have demonstrated that σ^0 was changed significantly depending on the correlation function.[34] Consequently, this parameter should be correctly calibrated to minimize the errors in the σ^0 modeling.[35–38] In this regard, several studies have calibrated the semiempirical IEM to improve its accuracy.[34,39] In these approaches, l was replaced by a calibration parameter called L^{opt}.[40]

The inversion of the IEM is not possible using analytical methods.[41,42] Thus several methods have inverted the corresponding equations to obtain surface parameters given the SAR parameters and the backscattering coefficient. These methods include lookup tables, artificial neural networks (ANN), Bayesian methods, minimization techniques,[43] support vector regression (SVR),[44] and multi-output SVR (MSVR).[45] The SVR, MSVR, and ANN are generally utilized to model complex relationships between input and output variables.[45,46] Furthermore, nonlinear relationships with high complexity can be modeled by these models.[47] SVR is a version of the support vector machine (SVM) that was first proposed in 1997 by Vapnik et al.[48] Tuia et al. (2011)[49] presented an implementation of the MSVR for remote sensing biophysical parameter estimation as an enhancement of SVR. MSVR allows predicting several output variables at once by sharing the same model parameters among all input parameters with the possibility of considering the relationship between output variables.[45,49] Moreover, MSVR significantly decreases the computation time by increasing the redundancy within output classes.[49] Several studies have applied the ANN, SVR, and MSVR to model the relationship between soil parameters and SAR configuration. For example, Ahmad et al.[50] estimated M_v using three machine learning approaches of the SVR, feed-forward ANN, and multivariate linear regression. The results

showed that the SVR model estimated M_v with higher accuracy. Moreover, Pasolli et al.[17] applied the SVR and ANN models to retrieve M_v using SAR data. The estimated soil moisture values from the two models were compared, and it was observed that the SVR model had a better accuracy. Additionally, Baghdadi et al.[51] investigated the potential of the polarimetric C-band SAR data for the soil surface parameters retrieval over agricultural fields. An ANN model was initially trained using a simulated dataset generated from the calibrated integral equation model (CIEM) and was then evaluated against the ground measurements and SAR datasets. The RMSEs of 7.0 vol. % and 0.5 cm were obtained for M_v and S, respectively. Furthermore, Baghdadi et al.[6] calibrated the WCM, in which the soil σ^0 depended on the soil and the SAR parameters were simulated using the CIEM. In this study, an ANN model employed for the inversion of the model[42] also investigated the performance of two radar backscattering models: the CIEM and the modified Dubois model (MDB). The CIEM and MDB performed with RMSEs of 0.78 and 1.45 dB, respectively. M_v was then retrieved using an ANN inversion method. The ANN model was trained using the simulated datasets generated from the CIEM and MDB. The inversion results showed that the single polarized data estimated M_v with a better accuracy. In addition,[45] the SVR and MSVR methods were used to invert the WCM using Sentinel-1 data. Mandal et al. in this research estimated the plant area index (PAI, $m^2\,m^{-2}$) and wet biomass (W, $kg\,m^{-2}$) from Sentinel-1 SAR data by inversion of the WCM, and the performance of the inversion method was also validated using *in situ* measurements. The validation results showed a good correlation for both wet biomass and PAI using the MSVR method. Finally, Ezzahar et al.[46] estimated M_v using the inversion of the IEM, OH, and SVM. The SAR data acquired over bare ground and *in situ* M_v were applied to assess the performance of the models. It was observed that the estimated M_v using σ^0_{VV} had a better accuracy compared to σ^0_{VH}. The maps produced by the SVM and IEM were similar and the RMSE of 2.77 and 2.71 vol. % were obtained from the SVM and IEM, respectively.

Most of the remote sensing studies have used a combination of optical and radar data to estimate soil parameters over vegetated agricultural areas. This has several limitations, such as the lack of suitable concurrent optical and SAR imagery or the existence of the cloud cover. Thus this study proposed a method to estimate M_v and S using only SAR data over vegetated agricultural areas. The first objective of this study was an investigation of the potential of machine learning techniques, such as SVR, MSVR, and ANN to model the relationship between SAR and soil parameters through the inversion method. The SAR parameters were simulated using the CIEM and parameterized WCM (PWCM). Additionally, we focused on the structures of the models to compare them with their inversion methods. The second and the main objective was estimating soil parameters over the vegetated agricultural areas by the trained models (i.e., SVR, MSVR, and ANN) using only Sentinel-1 SAR data (i.e., σ^0_{VV}, σ^0_{VH}, and θ). The main innovation of this study was to model soil parameters on the agricultural fields with vegetation cover using only SAR data utilizing the trained SVR, MSVR, and ANN without any vegetation describers derived from optical images as an input variable. Finally, the SMAP-VEX16-MB *in situ* dataset[52] was applied to perform the WCM parameterization and to evaluate the accuracy of the proposed method. In summary, after preprocessing the Sentinel-1 images, the WCM parameterization is implemented using 60% of the *in situ* dataset, in which the contribution from the soil in WCM was generated by the CIEM. Then 40% of the *in situ* dataset was applied to evaluate the WCM parameterization. After that, the SVR, MSVR, and ANN were used to invert the simulated dataset, which is generated by combination PWCM and CIEM. In the inversion process, the genetic algorithm (GA) is applied to optimize the models' parameters. Finally, the trained models applied to σ^0 and θ derived from Sentinel-1 data to evaluate the accuracy of the proposed method.

2 Study Area and Data

2.1 *Study Area*

The study area (Fig. 1) is near Winnipeg in Manitoba, Canada, with an area of 26 km × 48 km (latitude = 49.3°N to 49.8°N and longitude = 97.7°W to 98.2°W). The major crop types in this

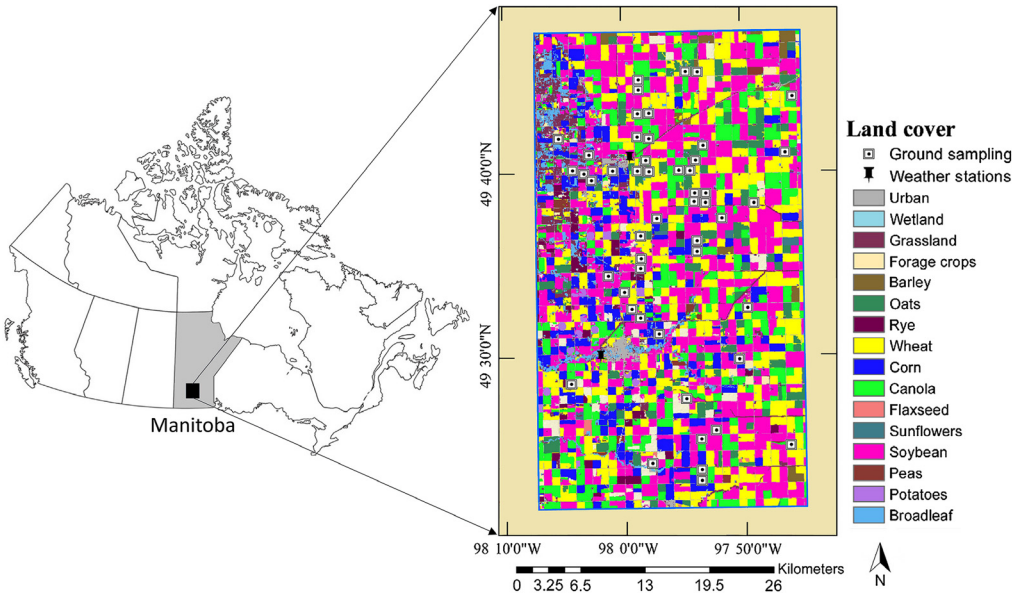

Fig. 1 Study area and land cover of the SMAPVEX16-MB ground campaign in Manitoba, Canada.[2]

area are corn, canola, wheat, winter wheat, oats, and soybeans (see the land cover map in Fig. 1). *In situ* measurements of crops and soil parameters were collected more than 50 agricultural fields from June 8, 2016, to July 22, 2016.

2.2 *Datasets*

In this section, three types of datasets are discussed: (1) the *in situ* datasets, which were used for the WCM parameterization and the evaluation of the proposed method; (2) satellite datasets; and (3) simulated dataset. All incorporated datasets are available in Ref. 53.

2.2.1 In situ *datasets*

Soil Moisture Active Passive Validation Experiment 2016 (SMAPVEX16-MB) datasets were measured in the field and are available in Ref. 54.[52] In this study, this *in situ* dataset was employed to develop and evaluate the proposed method. The SMAPVEX16-MB was conducted during the summer of 2016 and was focused on the monitoring of soil surface and crop. M_v, S, and VWC were mainly collected. In this study, M_v at the depth of 5 cm, S, and VWC collected on June 13, 2016, July 7, 2016, and July 19, 2016 were used for WCM parameterization and evaluation (Table 1). The *in situ* datasets were divided into three groups based on the VWC values to provide more reliable evaluation: (1) vegetation areas with VWC < 1.0 kg/m^2,

Table 1 The Sentinel-1 satellite images and *in situ* datasets, which were used in this study.

Date	θ (deg) [near–far]	# Field samples	M_v (vol. %) [min–max]	S (cm) [min–max]	VWC (kg/m^2) [min–max]
June 13, 2016	[29.2–31.8]	55	[10–35]	[0.33–2.07]	[0.002–1.9]
July 7, 2016	[37.4–39.6]	53	[7–62]		[0.026–3.56]
July 19, 2016	[31.5–33.9]	82	[14–51]		[0.042–4.92]

Note: θ, incidence angle; M_v, volumetric soil surface moisture; S, soil surface roughness; and VWC, vegetation water content.

(2) vegetation areas with VWC between 1.0 and 2.5 kg/m^2, and (3) vegetation areas with VWC > 2.5 kg/m^2. The distribution of the ground sites is shown in Fig. 1.

2.2.2 *Sentinel-1 datasets*

Three level-1 ground range detected Sentinel-1 images in the interferometric wide swath mode were used in this study. The images had a spatial resolution of 10 m in the dual-polarization (VH and VV) and were acquired in June and July 2016. Table 1 provides more information about these images. In this study, the imagery was initially multi-looked and ground-projected. Subsequently, they were preprocessed through radiometric calibration and terrain correction modules in the Sentinel-1 toolbox in the Sentinel Application Platform SNAP[55] to derive σ^0 and θ.

2.2.3 *Simulated datasets*

The simulated datasets were generated using the PWCM and CIEM; the methodology of this is discussed in Sec. 3.

3 Method

As discussed, the main objective of this study was to evaluate the sustainability of the SVR, MSVR, and ANN algorithms to model the relationship between SAR configuration and the soil parameters over vegetated agricultural areas. The flowchart of the proposed method is illustrated in Fig. 2 and is summarized in the following five steps. Additionally, the main steps of the proposed method are discussed in more detail in Secs. 3.1–3.3.

(1) The Sentinel-1 images were preprocessed to extract σ^0 and θ.
(2) The WCM was parameterized using the *in situ* datasets. The contribution from the soil in WCM was generated by the CIEM.
(3) The PWCM was evaluated against the *in situ* data and the extracted σ^0 values in the VV and VH polarizations.
(4) The GA was applied to optimize the parameters of the SVR, MSVR, and ANN algorithms through modeling the inversion of the simulated datasets.
(5) The performance of the proposed method for M_v and S retrieval was evaluated using the *in situ* datasets.

3.1 *Generating Simulated Dataset Using the WCM and CIEM*

The WCM has generally been applied to model the vegetation impacts on the backscattering coefficient over the vegetated agricultural areas. WCM computes two components: (1) the direct vegetation contribution and (2) the attenuation impacts on SAR backscattering using one vegetation descriptor that represents the vegetation effects.[5,56–58] In this model, the total backscattering value equals the vegetation backscatter and the soil backscatter with the attenuation coefficient. In this research, the WCM developed by Attema and Ulaby[59] was used [Eqs. (1)–(3)]:

$$\sigma^0_{\mathrm{tot},qp} = \sigma^0_{\mathrm{veg},qp} + T^2_{qp}\sigma^0_{\mathrm{soil},qp}, \tag{1}$$

$$\sigma^0_{\mathrm{veg},qp} = A_{qp}V_1 \cos\theta(1 - T^2_{qp}), \tag{2}$$

$$T^2_{qp} = e^{-2B_{qp}V_2 \sec\theta}, \tag{3}$$

where σ^0_{tot} is the backscattered radar signal, σ^0_{veg} is the backscattering component of the vegetation, σ^0_{soil} is the contribution from the soil, and qp determines the polarization type. T^2 is the two-way attenuation coefficient, V_1 and V_2 describe vegetation effects, θ is the incidence angle of the

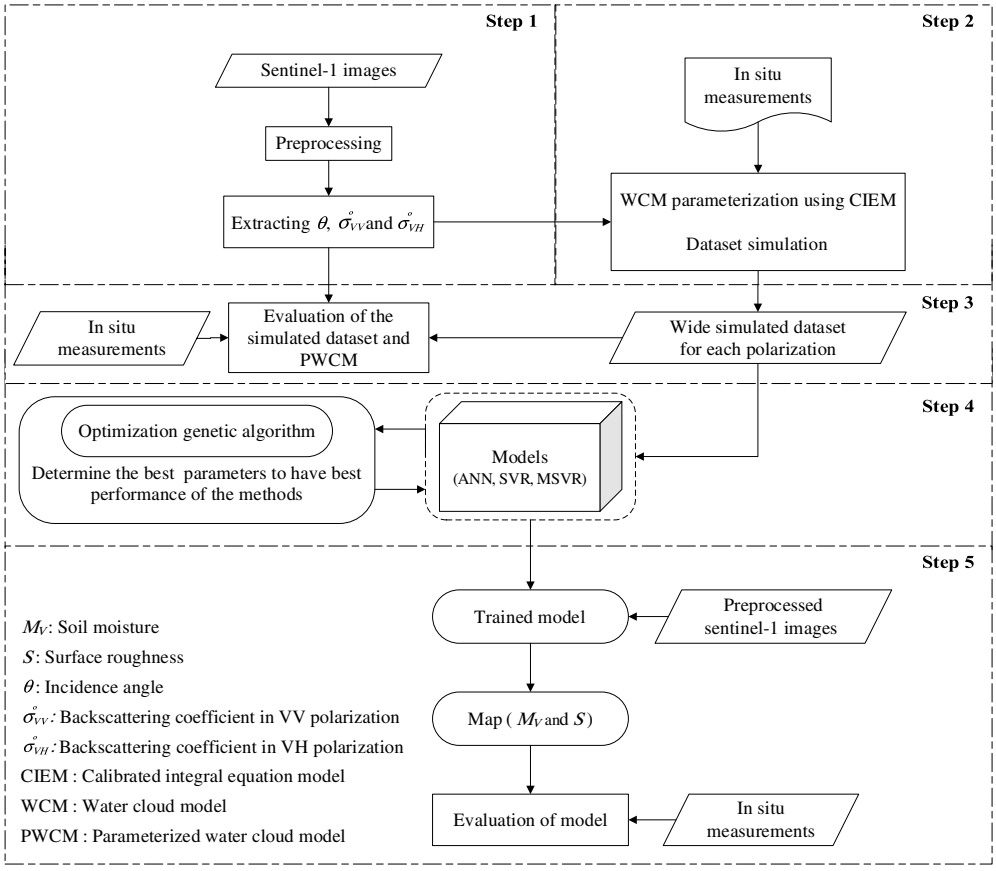

Fig. 2 Flowchart of the proposed method for estimating the soil surface parameters in vegetated agricultural areas based on the PWCM and the CIEM.

radar imaging geometry, and A_{qp}, and B_{qp} are WCM fitting parameters. In this study, σ^0_{soil} was generated using the CIEM and $V_1 = V_2 = \text{VWC}$.

3.2 *WCM Parameterization and Dataset Simulation*

The WCM parameters (A_{qp} and B_{qp}) were computed using 60% of the *in situ* dataset for Sentinel-1 VV and VH polarizations. For this, σ^0_{soil} was generated using the CIEM and *in situ* data for the input variables of the model. The 60% of *in situ* dataset were selected randomly. The rest of the *in situ* dataset (40%) was used to evaluate the performance of the WCM parameterization. The A_{qp} and B_{qp} were computed for both polarizations using the least-squares method.[3,5,6]

The PWCM was applied to generate a simulated dataset, where a range between 0 to 5 kg/m^2 was considered for VWC. This range was used to properly cover the characteristics of the land cover in the study area varying bare soil to vegetated regions. In this process, σ^0_{soil} as an input of the PWCM was simulated through the CIEM. The simulation process was performed by considering broad ranges of soil and SAR parameters as the inputs of the CIEM and PWCM to generate σ^0_{soil} (see Table 2). The values from the input variables were considered in a wider range compared to that of the ground measurements to represent more general situations.

The IEM has been semiempirically calibrated by Baghdadi et al.[39,60] In these studies, a fitting parameter (L^{opt}) was calculated as a function of θ, h_{rms}, polarization, and radar wavelength. By replacing L^{opt} with l in IEM, the IEM is changed to CIEM [see Eqs. (4) and (5) for the C-band]. In this study, the CIEM was applied to generate the simulated data.

$$L^{\text{opt}}_{\text{HV}}(h_{\text{rms}}, \theta) = 0.9157 + 1.2289\,(\sin 0.1543\,\theta)^{-0.3139} h_{\text{rms}}, \tag{4}$$

Table 2 The minimum, maximum, and step values of the PWCM and CIEM inputs to generate synthetic dataset.

Parameters (unit)	Min value	Step	Max value	Total elements
M_v (vol. %)	5	1	65	60
S (cm)	0.30	0.03	2.10	60
VWC (kg/m^2)	0	0.05	5	100
θ (deg)	29	0.1	34	50
	37	0.1	40	30
Total elements $= 60 \times 60 \times 100 \times (50 + 30) = 2.88 \times 10^{+7}$				

Note: θ, incidence angle; M_v, volumetric soil surface moisture; S, soil surface roughness; and VWC, vegetation water content.

$$L_{\mathrm{VV}}^{\mathrm{opt}}(h_{\mathrm{rms}}, \theta) = 1.281 + 0.134\,(\sin 0.19\,\theta)^{-1.59} h_{\mathrm{rms}}. \tag{5}$$

The simulated datasets were composed of $2.88 \times 10^{+7}$ elements. Table 2 presents the parameter boundaries and their steps, which were used to generate the simulated datasets. It is worth noting that the statistical parameters [e.g., RMSE, R^2, bias (estimated σ − measured σ), and standard deviation] were utilized to determine the efficiency of the simulated datasets and the WCM parameterization.

After co-registering the preprocessed Sentinel-1 SAR images and the *in situ* data, the simulated σ^0_{VV} and σ^0_{VH} corresponding to the field data were compared to σ^0 obtained from the Sentinel-1 data. Then the statistical parameters were calculated for accuracy assessment.

3.3 *Estimating Soil Parameters*

Machine learning algorithms have been utilized in many studies to model the complicated relationship between different variables that are physically related to each other.[50,61–65] In this study, the SVR, MSVR, and ANN were used to model the relationship between the simulated datasets, the soil parameters (output variables), and sensor variables (input variables).

3.3.1 *Soil surface parameters modeling using the simulated data*

ANNs can model the nonlinear relationships between complex and noisy datasets.[47] The ANNs' structures and processes have been explained by many studies.[62,66,67] In this study, a feed-forward ANN was used to develop the proposed model. SVR can be used for regression issues and has been widely applied to invert complicated models. The quality of an SVR model depends on the appropriate regulation of the modeling of SVR. Different types of SVR models have been effectively utilized for various inversion applications over the last two decades.[50,64] MSVR is another version of the SVR algorithm, which was proposed to model the relationships between multi-input parameters and multi-output parameters.[61]

In this study, the SVR, MSVR, and feed-forward ANN were trained separately using the simulated datasets, which were generated by the PWCM and CIEM. The MSVR and ANN used three-dimensional input vectors (σ^0_{VV}, σ^0_{VH}, and θ) and a two-dimensional output vector (M_v at the depth of 5 cm and S). According to the SVR structure, two separate models were trained for M_v and S retrieval. 25% of the simulated datasets were randomly applied to train the models and the rest were employed to evaluate the feasibility of the three methods to model the relationship between variables in the simulated datasets.

In the feed-forward ANN, several hidden layers were considered between the input and output layers. The Levenberg–Marquardt backpropagation algorithm[61] was utilized for finding the best weight and bias. The number of hidden layers and neurons were optimized by GA. The

kernels within the SVR and MSVR were used to reduce the complexity of the different issues. In this regard, the polynomial and radial basis function (RBF) kernels, which were commonly used,[68,69] were adopted. To obtain the SVR and MSVR with the highest performance, their parameters, regularization parameter (C), the RBF kernel width (γ), and loss function (ε) were optimized by the GA.

3.3.2 *Optimized GA parameters*

GA is an optimization method for solving problems based on natural selection that drives biological evolution. The structure and efficiency of this optimization algorithm have been discussed and evaluated in different studies.[70–73] The encodings of ANN parameters are binary. A range of [10 to 30] and [1 to 5] for the number of neurons in each layer and the number of hidden layers are, respectively, the optimum values according to Baghdadi et al.[51] Additionally, the SVR and MSVR parameters were encoded by real encoding. According to Pasolli et al.,[17] the ranges of space search for the GA were set to $[10^{-4}, 10^{+4}]$, $[10^{-5}, 10]$, and $[10^{-5}, 10]$ for C, γ, and ε, respectively. Moreover, the population size of GA was set to 50 to optimize the parameters.

4 Results and Discussion

4.1 *Evaluating Simulated Dataset and WCM Parameters*

The σ^0 values extracted from the Sentinel-1 images were compared with the simulated σ^0 values, which were generated by the CIEM and PWCM. 60% of the *in situ* datasets were randomly applied to parameterize WCM (A_{qp} and B_{qp} calculation) and to generate the simulated dataset. Table 3 shows the corresponding accuracies and the estimated values of A_{qp} and B_{qp} for each polarization. The rest of the *in situ* datasets were divided into three groups to evaluate the accuracy of the parameterization and simulated dataset for different VWC values (Fig. 3).

The results demonstrated that the efficiency of the PWCM was similar in both polarizations. For instance, as VWC increases, RMSE, bias, and StDv increase and R^2 decreases in the estimation of both polarizations (Fig. 3). According to Fig. 3, PWCM produced the simulated datasets that were closer to σ^o with VWC lower than 2.5 kg/m^2. However, the accuracy of the PWCM was relatively decreased for VWC higher than 2.5 kg/m^2 in the VV and VH polarizations. The accuracy of the model for the estimation of σ^0 in the VV polarization was better than that of the VH polarization. However, the model estimation was not generally reliable for VWC higher than 2.5 kg/m^2. The R^2 values for all validation datasets were equal to 54.7% and 50.4% in the VV and VH polarizations, respectively. The RMSE values were also equal to 2.35 and 2.45 dB in these polarizations, respectively. The bias values for all validation datasets were <0.4 dB. According to the WCM parameterization accuracy (Table 3), the simulated datasets were not reliable when VWC was higher than 2.5 kg/m^2, however, it can be effectively used for VWC lower than 2.5 kg/m^2. The WCM parameterization was considered adequately fitted for VWC < 2.5 kg/m^2. In this case, the RMSE values on the simulated datasets in both VV and VH polarization were <2 dB and with a bias lower than 0.4 dB. In comparison with the Sentinel-1,[6,8] used Sentinel-1 data and showed that the WCM estimates σ^0 with an RMSE of higher than 1.5 dB. Results show standard deviations lower than 2 dB for the VWC lower than 2.5 kg/m^2.

4.2 *GA Algorithm Results*

The GA algorithm was applied to optimize the parameters of the ANN, SVR, and MSVR. The SVR and MSVR parameters (C, γ, and ε) reached an optimal solution approximately at the 50th generation of the algorithm, and the ANN parameters were optimized at the 60th generation. The optimized SVR and MSVR parameters and the optimized ANN parameters are provided in Table 4.

Table 3 WCM parameterization for each polarization (VV and VH) using the training dataset (VWC is in kg/m^2).

		$qp = \mathrm{VV}$	$qp = \mathrm{VH}$	
	Polarization	$A_{qp} = 0.0428$, $B_{qp} = 0.0961$	$A_{qp} = 0.091$, $B_{qp} = 0.1994$	
VWC < 1	RMSE (vol. %)	1.44	1.77	$T = 21$
	R^2 (%)	74.8	67.7	
	Bias (vol. %)	–0.31	0.39	
	StDv (vol. %)	1.44	1.77	
1 < VWC < 2.5	RMSE (vol. %)	1.88	1.97	$T = 18$
	R^2 (%)	68.4	64.5	
	Bias (vol. %)	–0.34	–0.23	
	StDv (vol. %)	1.90	2.02	
2.5 < VWC	RMSE (vol. %)	2.91	2.95	$T = 36$
	R^2 (%)	39.6	20.2	
	Bias (vol. %)	–0.28	0.35	
	StDv (vol. %)	2.94	2.97	
Overall accuracy	RMSE (vol. %)	2.35	2.45	$N = 115$, $T = 75$
	R^2 (%)	54.7	50.4	
	Bias (vol. %)	–0.30	0.22	
	StDv (vol. %)	2.34	2.45	

Note: N is the number of samples used in the model fitting and T is the number of samples used to evaluate the accuracy of the models. A_{qp} and B_{qp} are the WCM parameters.

4.3 *Accuracy Assessment of the Proposed Method for Simulation Dataset*

After parameterization of the WCM and generating the simulation datasets, 25% of the simulated datasets were randomly applied to train the SVR, MSVR, and ANN machine learning algorithms to model the relationship between the input variables (σ^0_{VV}, σ^0_{VH}, and θ) and output variables (M_v and S). The rest of the simulated dataset was utilized to evaluate the accuracy of the models. Table 4 provides the performance of the SVR, MSVR, and ANN to model the relationship between variables in the simulated datasets. All methods have reasonably modeled the relationship between the variables of the simulated dataset. In this regard, the ANN and MSVR algorithms had better results compared to those of SVR. According to the ANN and MSVR structures, they can estimate that multiple output variables can consider the relationship between the output variables. Thus they can model the inversion of the PWCM and CIEM with better accuracy by considering all relationships between variables. However, since the SVR estimates only a single output, it could not efficiently consider the relationship between the output variables.

4.4 *Accuracy Assessment of the Proposed Method for M_v and S Estimation*

The estimated M_v and S using the trained SVR, MSVR, and ANN were compared with the *in situ* data. The algorithm was separately applied to the three subdatasets (i.e., different VWC values), where the corresponding accuracies are provided in Table 5. Figures 4 and 5 also illustrate the regression graphs between *in situ* data and the estimated M_v and S.

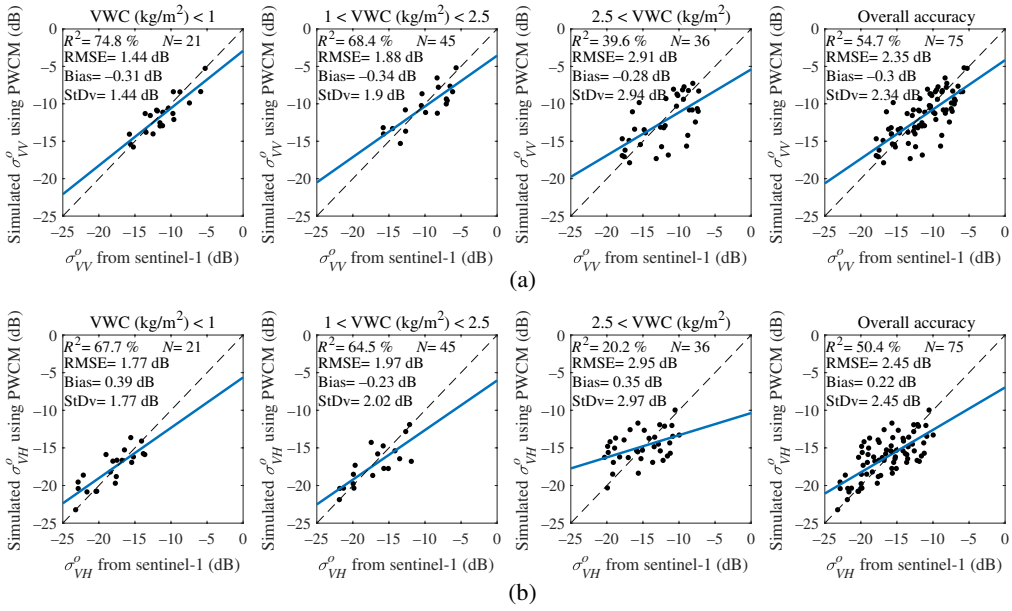

Fig. 3 The regression between the σ^0 values extracted from the Sentinel-1 images and the σ^0 values simulated using the PWCM and CIEM in (a) VV and (b) VH polarizations (VWC: vegetation water content, RMSE, R^2, bias: mean(estimated σ – measured σ), and StDv: standard deviation).

According to Figs. 4, 5, and Table 5, the performances of the trained ANN and MSVR algorithms were approximately similar and were better than that of the trained SVR algorithm. According to Table 5, the most accurate results for estimating both M_v and S were obtained when VWC was <1.0 kg/m^2. The results were also reasonable when VWC was <2.5 kg/m^2. However, the estimation of both M_v and S for VWC > 2.5 kg/m^2 was unreliable and had a low correlation with the *in situ* measurements. According to the WCM parameterization evaluation, the parameterization and models' estimation behaved similarly for different VWC values. The results of the WCM parameterization and the trained models showed that the sensitivity of σ^0 to the soil, parameters were reduced when VWC was >2.5 kg/m^2. This result corresponds well to those of other studies such as Refs. 3 and 5.

Comparing the three models, the trained MSVR and ANN algorithms modeled the relationships between SAR and soil parameters (M_v and S) better than SVR due to their structures. The SVR does not consider relationships between output variables (M_v and S) and, therefore, could not accurately invert the combination of PWCM and CIEM. According to the MSVR and ANN structures, the physical relationships between all input and output variables can be accurately

Table 4 The most optimal parameters for the models along with their accuracies to model the relationship between simulated dataset variables.

					M_v		S	
		C	γ	ε	RMSE (vol. %)	R^2 (%)	RMSE (cm)	R^2 (%)
SVR	M_v	8218.9	0.935512	0.110785	1.92	98.3		
	S	3580.2	0.445696	0.047903			0.095	98.5
MSVR		6801.5	0.860418	0.079486	1.42	99.1	0.053	99.6
ANN		NLayer(NNeuron)			1.72	98.7	0.063	99.2
		3 (22, 22, 20)						

Note: C, regularization parameter; γ, the RBF kernel width; ε, loss function; NLayer, the number of ANN hidden layers; and NNeuron, the number of neurons in each layer.

Table 5 The performance of the models to estimate soil parameters (VWC is in kg/m^2). T is the number of test samples used to evaluate the accuracy of the models.

		M_v			S			
		SVR	MSVR	ANN	SVR	MSVR	ANN	
VWC < 1	RMSE (vol. %)	5.24	4.57	4.70	0.4	0.350	0.360	$T = 58$
	R^2 (%)	68.4	76.7	75.5	58.6	68.9	66.2	
	Bias (vol. %)	−0.520	0.430	−0.970	−0.07	−0.09	0	
	StDv (vol. %)	5.26	4.59	4.64	0.4	0.340	0.370	
1 < VWC < 2.5	RMSE (vol. %)	6.48	7.18	6.26	0.460	0.420	0.420	$T = 45$
	R^2 (%)	63.8	64.9	66.3	53.7	61.9	60.9	
	Bias (vol. %)	1.02	−3	0.470	−0.07	−0.06	0.01	
	StDv (vol. %)	6.47	6.60	6.32	0.460	0.420	0.420	
2.5 < VWC	RMSE (vol. %)	8.89	9.01	9.21	0.480	0.460	0.510	$T = 87$
	R^2 (%)	30.7	27.3	26.8	33.6	35.5	29.6	
	Bias (vol. %)	0.360	0.580	1.75	−0.05	0.01	0.1	
	StDv (vol. %)	8.94	9.04	9.10	0.480	0.460	0.5	
Overall accuracy	RMSE (vol. %)	10.04	7.04	7.16	0.610	0.460	0.480	$T = 190$
	R^2 (%)	39.7	54.8	53.1	25.3	46.8	44	
	Bias (vol. %)	−6.20	−0.36	−0.08	−0.240	−0.04	0.01	
	StDv (vol. %)	7.92	7.05	7.18	0.560	0.460	0.490	

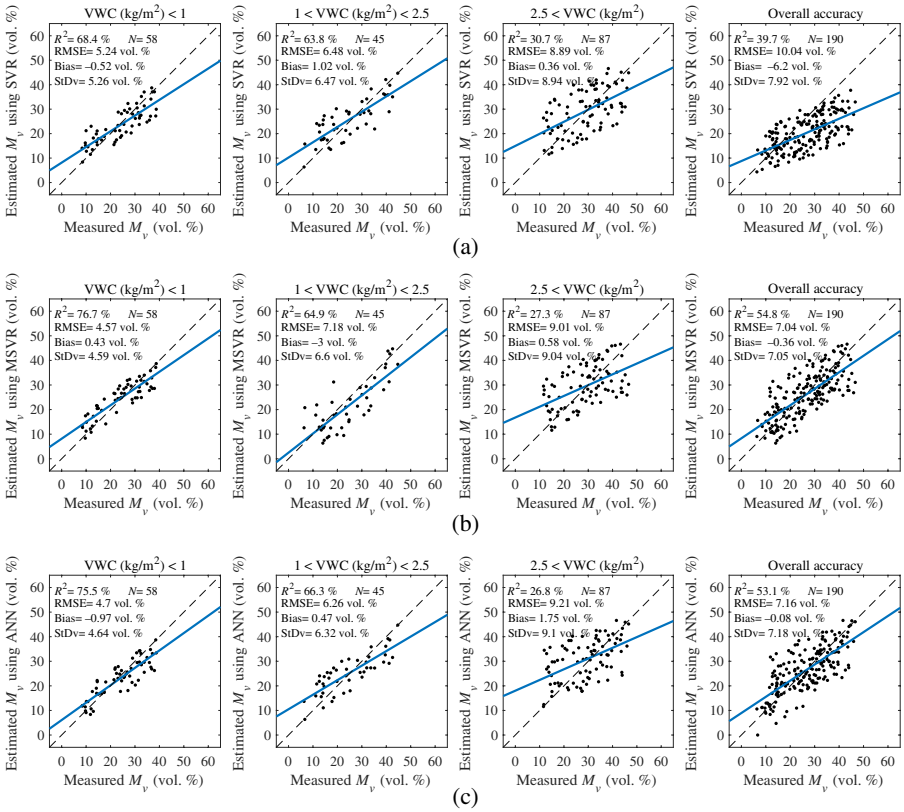

Fig. 4 Comparison between the *in situ* M_v and the estimated M_v using the trained: (a) SVR; (b) MSVR; and (c) ANN algorithms.

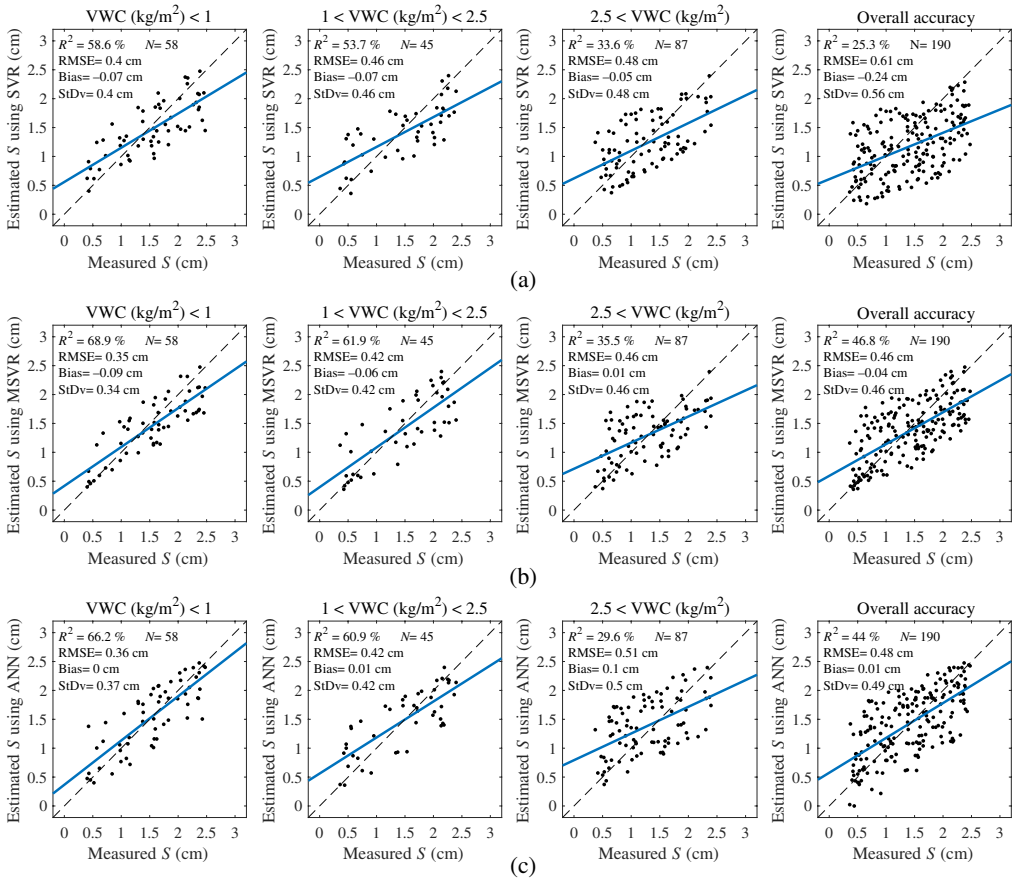

Fig. 5 Comparison between the *in situ S* and the estimated *S* using the trained: (a) SVR; (b) MSVR; and (c) ANN algorithms.

modeled. It is worth noting that these results correspond well with those of several studies such as Refs. 74 and 75. In summary, the multi-output algorithms (e.g., MSVR and ANN) could invert a combination of the PWCM and CIEM with better accuracy. Additionally, the proposed method's efficiency to estimate M_v and S using a combination of PWCM and CIEM with only Sentinel-1 image was reduced over vegetated agricultural areas with VWC > 2.5 kg/m^2. There were two main reasons for this: (1) the sensitivity of σ^0 to M_v and S reduces over the

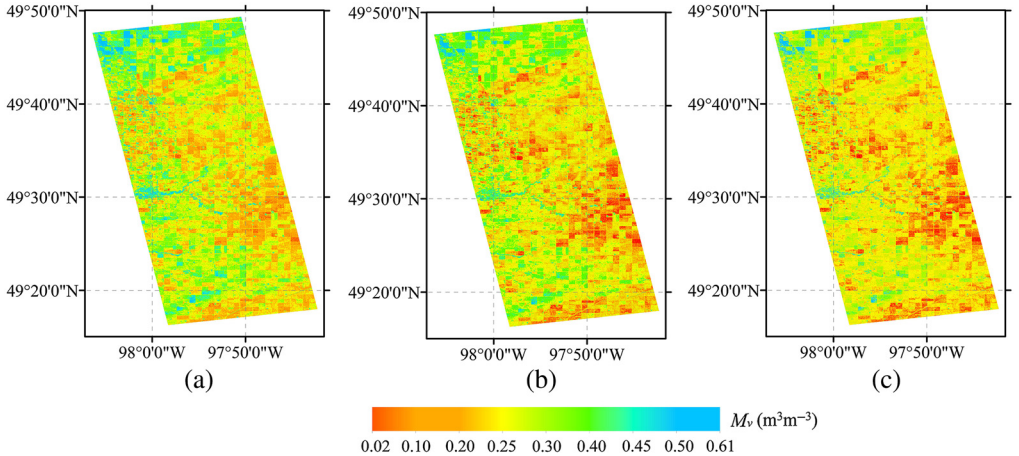

Fig. 6 Estimated soil moisture (M_v) using the trained: (a) SVR; (b) MSVR; and (c) ANN algorithms. The Sentinel-1 image was acquired on July 7, 2016.

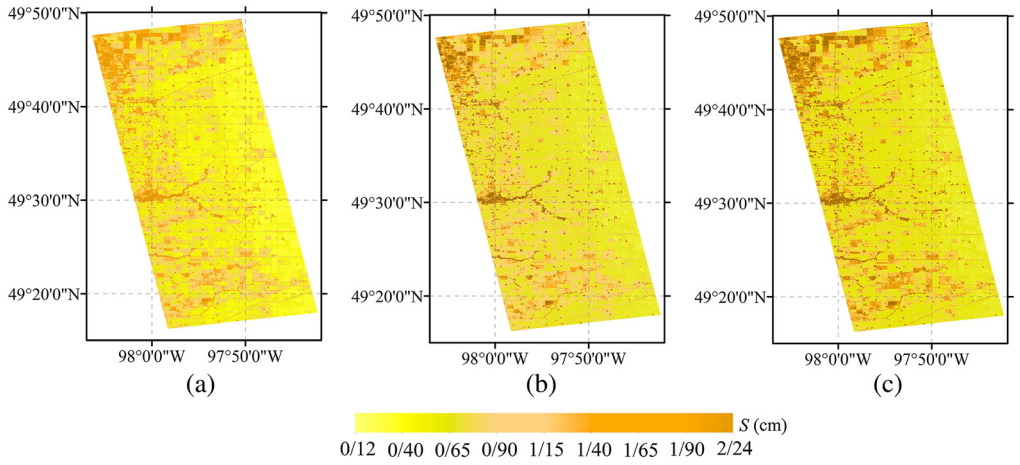

Fig. 7 Estimated soil roughness (S) using the trained: (a) SVR; (b) MSVR; and (c) ANN algorithms. The Sentinel-1 image was captured on July 7, 2016.

vegetation areas with VWC > 2.5 kg/m^2 and (2) the PWCM cannot accurately model the total backscattered radar signal when VWC is >2.5 kg/m^2.

After evaluating the proposed methods' accuracy, the trained machine learning algorithms were applied to the Sentinel-1 SAR image acquired on July 7, 2016 to retrieve M_v and S (see Figs. 6 and 7). According to Figs. 6(b) and 6(c), the results of the trained MSVR and ANN were similar and the estimated M_v using these models were not very different. However, the result of the SVR for M_v estimation was different from those of the other two models. Similar results were also observed when the models were compared to estimate S (see Fig. 7).

5 Conclusions

This study investigated the potential of the three machine learning algorithms (feed-forward ANN, SVR, and MSVR) to invert a combination of PWCM and CIEM using only Sentinel-1 SAR images to map M_v and S. Based on the results of the WCM parameterization, this model could estimate VV and VH polarizations in the C-band with acceptable accuracies for VWC < 2.5 kg/m^2. Inversion results of the simulated datasets showed that the best results for M_v and S estimation were obtained from the trained MSVR and ANN because of their structures. Additionally, better results were obtained for vegetated agricultural areas with VWC < 2.5 kg/m^2. This study showed that M_v and S can be estimated with reasonable accuracy when VWC is <2.5 kg/m^2 (RMSE $=$ 4 to 7 vol. % and 0.35 to 0.46 cm depending on the VWC values for M_v and S, respectively). Current remote sensing SAR sensors (such as Sentinel-1 with 10-m spatial resolution) enable researchers to estimate soil parameters with high spatial and temporal resolutions. Finally, this study's results demonstrated that soil parameters can be effectively retrieved with a machine learning inversion method and with the sole use of SAR data for VWC < 2.5 kg/m^2.

Acknowledgments

The authors would like to thank all the SMAPVEX16-MB campaign members for collecting and providing these valuable datasets and ESA for providing these datasets. The Sentinel-1 datasets are also available through Copernicus Open Access Hub.

References

1. N. Baghdadi and M. Zribi, "Evaluation of radar backscatter models IEM, OH and Dubois using experimental observations," *Int. J. Remote Sens.* **27**(18), 3831–3852 (2006).

2. H. Wang et al., "Crop phenology retrieval via polarimetric SAR decomposition and random forest algorithm," *Remote Sens. Environ.* **231**, 111234 (2019).
3. M. El Hajj et al., "Synergic use of Sentinel-1 and Sentinel-2 images for operational soil moisture mapping at high spatial resolution over agricultural areas," *Remote Sens.* **9**(12), 1292 (2017).
4. R. Panciera et al., "Evaluation of IEM, Dubois, and Oh radar backscatter models using airborne L-band SAR," *IEEE Trans. Geosci. Remote Sens.* **52**(8), 4966–4979 (2014).
5. M. El Hajj et al., "Soil moisture retrieval over irrigated grassland using X-band SAR data," *Remote Sens. Environ.* **176**, 202–218 (2016).
6. N. Baghdadi et al., "Calibration of the water cloud model at C-band for winter crop fields and grasslands," *Remote Sens.* **9**(9), 969 (2017).
7. M. C. Dobson and F. T. Ulaby, "Active microwave soil moisture research," *IEEE Trans. Geosci. Remote Sens.* **GE-24**(1), 23–36 (1986).
8. M. El Hajj et al., "Analysis of Sentinel-1 radiometric stability and quality for land surface applications," *Remote Sens.* **8**(5), 406 (2016).
9. S. M. Mirmazloumi, M. R. Sahebi, and M. Amani, "New empirical backscattering models for estimating bare soil surface parameters," *Int. J. Remote Sens.* **42**(5), 1928–1947 (2021).
10. P. C. Dubois, J. Van Zyl, and T. Engman, "Measuring soil moisture with imaging radars," *IEEE Trans. Geosci. Remote Sens.* **33**(4), 915–926 (1995).
11. A. K. Fung, Z. Li, and K.-S. Chen, "Backscattering from a randomly rough dielectric surface," *IEEE Trans. Geosci. Remote Sens.* **30**(2), 356–369 (1992).
12. Y. Oh, K. Sarabandi, and F. T. Ulaby, "An empirical model and an inversion technique for radar scattering from bare soil surfaces," *IEEE Trans. Geosci. Remote Sens.* **30**(2), 370–381 (1992).
13. M. R. Sahebi and J. Angles, "An inversion method based on multi-angular approaches for estimating bare soil surface parameters from RADARSAT-1," *Hydrol. Earth Syst. Sci.* **14**(11), 2355 (2010).
14. S. Esch et al., "Soil moisture index from ERS-SAR and its application to the analysis of spatial patterns in agricultural areas," *J. Appl. Remote Sens.* **12**(2), 022206 (2018).
15. F. T. Ulaby et al., "Michigan microwave canopy scattering model," *Int. J. Remote Sens.* **11**(7), 1223–1253 (1990).
16. M. Zribi et al., "New methodology for soil surface moisture estimation and its application to ENVISAT-ASAR multi-incidence data inversion," *Remote Sens. Environ.* **96**(3–4), 485–496 (2005).
17. L. Pasolli, C. Notarnicola, and L. Bruzzone, "Estimating soil moisture with the support vector regression technique," *IEEE Geosci. Remote Sens. Lett.* **8**(6), 1080–1084 (2011).
18. A. Ghafouri et al., "Better estimated IEM input parameters using random fractal geometry applied on multi-frequency SAR data," *Remote Sens.* **9**(5), 445 (2017).
19. J. Shi et al., "Estimation of bare surface soil moisture and surface roughness parameter using L-band SAR image data," *IEEE Trans. Geosci. Remote Sens.* **35**(5), 1254–1266 (1997).
20. N. Baghdadi et al., "A new empirical model for radar scattering from bare soil surfaces," *Remote Sens.* **8**(11), 920 (2016).
21. G. Satalino et al., "On current limits of soil moisture retrieval from ERS-SAR data," *IEEE Trans. Geosci. Remote Sens.* **40**(11), 2438–2447 (2002).
22. S. M. MirMazloumi and M. R. Sahebi, "Assessment of different backscattering models for bare soil surface parameters estimation from SAR data in band C, L and P," *Eur. J. Remote Sens.* **49**(1), 261–278 (2016).
23. M. Zribi and M. Dechambre, "A new empirical model to retrieve soil moisture and roughness from C-band radar data," *Remote Sens. Environ.* **84**(1), 42–52 (2003).
24. J. B. Boisvert et al., "Effect of surface soil moisture gradients on modelling radar backscattering from bare fields," *Int. J. Remote Sens.* **18**(1), 153–170 (1997).
25. A. Ghafouri et al., "Measuring the surface roughness of geological rock surfaces in SAR data using fractal geometry," *Comptes Rendus Geosci.* **349**(3), 114–125 (2017).
26. B. He, M. Xing, and X. Bai, "A synergistic methodology for soil moisture estimation in an alpine prairie using radar and optical satellite data," *Remote Sens.* **6**(11), 10966–10985 (2014).

27. S. Mahdavi, Y. Maghsoudi, and S. Dehnavi, "A method for soil moisture retrieval in vegetated areas using multi-frequency data considering different kinds of interaction in different frequencies," in *10th Eur. Conf. Syn. Aperture Radar*, VDE, pp. 1–4 (2014).
28. N. Chen et al., "Surface soil moisture estimation at high spatial resolution by fusing synthetic aperture radar and optical remote sensing data," *J. Appl. Remote Sens.* **14**(2), 024508 (2020).
29. I. Gherboudj et al., "Soil moisture retrieval over agricultural fields from multi-polarized and multi-angular RADARSAT-2 SAR data," *Remote Sens. Environ.* **115**(1), 33–43 (2011).
30. E. Khedri, M. Hasanlou, and A. Tabatabaeenejad, "Semi-analytical soil moisture retrieval using PolSAR imagery," in *IEEE Int. Geosci. and Remote Sens. Symp.*, IEEE, pp. 4897–4900 (2017).
31. Y. Bao et al., "Surface soil moisture retrievals over partially vegetated areas from the synergy of Sentinel-1 and Landsat 8 data using a modified water-cloud model," *Int. J. Appl. Earth Obs. Geoinf.* **72**, 76–85 (2018).
32. M. Xing et al., "Retrieving surface soil moisture over wheat and soybean fields during growing season using modified water cloud model from RADARSAT-2 SAR data," *Remote Sens.* **11**(16), 1956 (2019).
33. K. S. Rawat, S. K. Singh, and R. K. Pal, "Synergetic methodology for estimation of soil moisture over agricultural area using Landsat-8 and Sentinel-1 satellite data," *Remote Sens. Appl. Soc. Environ.* **15**, 100250 (2019).
34. N. Baghdadi et al., "Semi-empirical calibration of the integral equation model for co-polarized L-band backscattering," *Remote Sens.* **7**(10), 13626–13640 (2015).
35. N. Baghdadi et al., "Semi-empirical calibration of the IEM backscattering model using radar images and moisture and roughness field measurements," *Int. J. Remote Sens.* **25**(18), 3593–3623 (2004).
36. M. Zribi et al., "Characterisation of the soil structure and microwave backscattering based on numerical three-dimensional surface representation: analysis with a fractional Brownian model," *Remote Sens. Environ.* **72**(2), 159–169 (2000).
37. Y. Oh and Y. C. Kay, "Condition for precise measurement of soil surface roughness," *IEEE Trans. Geosci. Remote Sens.* **36**(2), 691–695 (1998).
38. N. Baghdadi et al., "Relationship between profile length and roughness variables for natural surfaces," *Int. J. Remote Sens.* **21**(17), 3375–3381 (2000).
39. N. Baghdadi, N. Holah, and M. Zribi, "Calibration of the integral equation model for SAR data in C-band and HH and VV polarizations," *Int. J. Remote Sens.* **27**(4), 805–816 (2006).
40. N. Baghdadi, J. A. Chaaya, and M. Zribi, "Semiempirical calibration of the integral equation model for SAR data in C-band and cross polarization using radar images and field measurements," *IEEE Geosci. Remote Sens. Lett.* **8**(1), 14–18 (2011).
41. K. G. Zhao et al., "Retrieval of bare soil surface parameters from simulated data using neural networks combined with IEM," in *IEEE Int. Geosci. and Remote Sens. Symp. Proc. (IEEE Cat. No. 03CH37477)*, IEEE, Vol. 6, pp. 3881–3883 (2003).
42. H. R. Mirsoleimani et al., "Bare soil surface moisture retrieval from sentinel-1 SAR data based on the calibrated IEM and Dubois models using neural networks," *Sensors* **19**(14), 3209 (2019).
43. B. W. Barrett, E. Dwyer, and P. Whelan, "Soil moisture retrieval from active spaceborne microwave observations: an evaluation of current techniques," *Remote Sens.* **1**(3), 210–242 (2009).
44. C. Zhihui et al., "Inversion of soil moisture from backscattering coefficient using LS-SVM," in *Int. Conf. Remote Sens., Environ. and Transp. Eng.*, Atlantis Press (2013).
45. D. Mandal et al., "Crop biophysical parameter retrieval from Sentinel-1 SAR data with a multi-target inversion of Water Cloud Model," *Int. J. Remote Sens.* **41**(14), 5503–5524 (2020).
46. J. Ezzahar et al., "Evaluation of backscattering models and support vector machine for the retrieval of bare soil moisture from Sentinel-1 data," *Remote Sens.* **12**(1), 72 (2020).
47. N. K. C. Twarakavi, D. Misra, and S. Bandopadhyay, "Prediction of arsenic in bedrock derived stream sediments at a gold mine site under conditions of sparse data," *Nat. Resour. Res.* **15**(1), 15–26 (2006).

48. V. Vapnik, S. E. Golowich, and A. J. Smola, "Support vector method for function approximation, regression estimation and signal processing," in *Adv. Neural Inf. Process. Syst.*, pp. 281–287 (1997).
49. D. Tuia et al., "Multioutput support vector regression for remote sensing biophysical parameter estimation," *IEEE Geosci. Remote Sens. Lett.* **8**(4), 804–808 (2011).
50. S. Ahmad, A. Kalra, and H. Stephen, "Estimating soil moisture using remote sensing data: a machine learning approach," *Adv. Water Resour.* **33**(1), 69–80 (2010).
51. N. Baghdadi et al., "Estimation of soil parameters over bare agriculture areas from C-band polarimetric SAR data using neural networks," *Hydrol. Earth Syst. Sci.* **16**(6), 1607–1621 (2012).
52. H. McNairn et al., "SMAPVES-16 experimental plan," pp. 1–71 (2016).
53. M. Hasanlou, "Remote sensing lab," University of Tehran, https://rslab.ut.ac.ir/data (2021).
54. H. Mcnairn, K. Gottfried, and J. Powers, "SMAPVEX16 manitoba station soil moisture data, Version 1," NASA National Snow and Ice Data Center Distributed Active Archive Center (2018).
55. M. Foumelis, "ESA snap Sentinel-1 toolbox" (2017).
56. M. Zribi et al., "Soil surface moisture estimation over a semi-arid region using ENVISAT ASAR radar data for soil evaporation evaluation," *Hydrol. Earth Syst. Sci. Discuss.* **15**(1), 345–358 (2011).
57. S. Paloscia et al., "Soil moisture mapping using Sentinel-1 images: algorithm and preliminary validation," *Remote Sens. Environ.* **134**, 234–248 (2013).
58. M. Hosseini and M. R. Saradjian, "Soil moisture estimation based on integration of optical and SAR images," *Can. J. Remote Sens.* **37**(1), 112–121 (2011).
59. E. P. W. Attema and F. T. Ulaby, "Vegetation modeled as a water cloud," *Radio Sci.* **13**(2), 357–364 (1978).
60. N. Baghdadi, J. A. Chaaya, and M. Zribi, "Semiempirical calibration of the integral equation model for SAR data in C-Band and cross polarization using radar images and field measurements," *IEEE Geosci. Remote Sens. Lett.* **8**(1), 14–18 (2011).
61. Y. Zhou et al., "Multi-output support vector machine for regional multi-step-ahead PM2. 5 forecasting," *Sci. Total Environ.* **651**, 230–240 (2019).
62. C. M. Zealand, D. H. Burn, and S. P. Simonovic, "Short term streamflow forecasting using artificial neural networks," *J. Hydrol.* **214**(1–4), 32–48 (1999).
63. D. W. Marquardt, "An algorithm for least-squares estimation of nonlinear parameters," *J. Soc. Ind. Appl. Math.* **11**(2), 431–441 (1963).
64. E. Khedri, M. Hasanlou, and A. Tabatabaeenejad, "Estimating soil moisture using polsar data: a machine learning approach," *Int. Arch. Photogramm. Remote Sens. Spatial Inf. Sci.* **XLII-4/W4**, 133–137 (2017).
65. R. Chandra, Y.-S. Ong, and C.-K. Goh, "Co-evolutionary multi-task learning with predictive recurrence for multi-step chaotic time series prediction," *Neurocomputing* **243**, 21–34 (2017).
66. K. Hsu, H. V. Gupta, and S. Sorooshian, "Artificial neural network modeling of the rainfall-runoff process," *Water Resour. Res.* **31**(10), 2517–2530 (1995).
67. S. Ahmad and S. P. Simonovic, "An artificial neural network model for generating hydrograph from hydro-meteorological parameters," *J. Hydrol.* **315**(1–4), 236–251 (2005).
68. L. Bruzzone and F. Melgani, "Robust multiple estimator systems for the analysis of biophysical parameters from remotely sensed data," *IEEE Trans. Geosci. Remote Sens.* **43**(1), 159–174 (2005).
69. M. Hasanlou, F. Samadzadegan, and S. Homayouni, "SVM-based hyperspectral image classification using intrinsic dimension," *Arab. J. Geosci.* **8**(1), 477–487 (2015).
70. S. K. Pal and P. P. Wang, *Genetic Algorithms for Pattern Recognition*, CRC Press, Boca Raton, Florida (2017).
71. O. Kramer, "Genetic algorithms," in *Genetic Algorithm Essentials*, pp. 11–19, Springer, Berlin, Germany (2017).
72. P. Ghamisi and J. A. Benediktsson, "Feature selection based on hybridization of genetic algorithm and particle swarm optimization," *IEEE Geosci. Remote Sens. Lett.* **12**(2), 309–313 (2015).

73. S. D. Dao, K. Abhary, and R. Marian, "An innovative framework for designing genetic algorithm structures," *Expert Syst. Appl.* **90**, 196–208 (2017).
74. L. Zhao et al., "Feature constrained multi-task learning models for spatiotemporal event forecasting," *IEEE Trans. Knowl. Data Eng.* **29**(5), 1059–1072 (2017).
75. T. Shireen et al., "Iterative multi-task learning for time-series modeling of solar panel PV outputs," *Appl. Energy* **212**, 654–662 (2018).

Sadegh Ranjbar received his BS degree in surveying and geomatics engineering from the Faculty of Civil Engineering at Shaheed Rajaei Teacher Training University in 2017 and his MS degree in remote sensing from the College of Engineering at the University of Tehran in 2021. His research interests include analyzing different remote sensing datasets through AI and ML approaches for urban and agro-environmental applications.

Arastou Zarei received his BS degree in surveying and geomatics engineering from the University of Tabriz, Tabriz, Iran, in 2017. He is currently a student of remote sensing at the University of Tehran. His research interests include remote sensing and image analysis, focusing on advanced machine learning approaches, multisensor data regression, and SAR remote sensing.

Mahdi Hasanlou received his BSc degree in surveying and geomatics engineering, and his MSc and PhD degrees in remote sensing from the University of Tehran, Tehran, Iran, in 2003, 2006, and 2013, respectively. Since 2013, he has been an assistant professor at the School of Surveying and Geospatial Engineering, College of Engineering, University of Tehran, Tehran, Iran, where he is the head of the Remote Sensing Laboratory. He is currently the head of the Remote Sensing and Photogrammetry Group at this school. His research activities are mainly focused on hyperspectral, thermal, optical, and SAR remote sensing for urban and agro-environmental applications.

Mehdi Akhoondzadeh received his BSc degree in civil-surveying engineering from Amirkabir University of Technology, and his MSc and PhD degrees in civil-remote sensing engineering from the University of Tehran, in 2002, 2005, and 2011, respectively. He is currently an assistant professor at the School of Surveying and Geo-Spatial Engineering of the College of Engineering at the University of Tehran. His research interests include the applied remote sensing, soft computing, time series analysis, anomaly detection, and earthquake precursors.

Jalal Amini is a professor in microwave remote sensing at the School of Geo-Spatial Engineering of the University of Tehran. He is also the director of the Microwave Remote Sensing Laboratory (MReSL) at the same university. His activities at the MReSL include: SAR signal processing, SAR polarimetric image analysis with applications, and ground-based SAR sensor designing.

Meisam Amani received his BEng degree in geomatics engineering from the University of Tabriz in 2012, his MEng degree in remote sensing engineering from K.N. Toosi University of Technology in 2014, and his PhD in electrical engineering from the Memorial University of Newfoundland in 2018. He is currently a senior remote sensing engineer and the key specialty leader of data analytics at a global consulting and engineering company, called Wood PLC, where he manages and leads various industrial, governmental, and academic remote sensing projects worldwide. He is an associate editor in IEEE JSTARS and the lead guest editor for a special issue in the *Remote Sensing Journal*. He also serves as a regular reviewer in about 15 international remote sensing journals. He has received the prestigious Professional Engineers and Geoscientists Newfoundland and Labrador Environmental Award in 2020 due to his contribution to wetland mapping in Canada using advanced machine learning and big data processing algorithms.